Chapter 7

Large scale shell model calculations in Ni region: ^{40}Ca as a core

In this chapter, large scale shell model calculations have been performed for neutron rich nickel, copper and zinc isotopes with $40 \leq N \leq 50$ using ^{40}Ca as a core by including the $f_{7/2}$ orbit. In the previous chapter large scale shell model calculations were performed for neutron rich nickel, copper and zinc isotopes for $40 \leq N \leq 50$, using two different versions [Lis04] [Now96] [Smi04] of effective interactions for the model space consisting of the $p_{3/2}$, $p_{1/2}$, $f_{5/2}$ and $g_{9/2}$. Both, however, yield unsatisfactory results in certain aspects, viz.
(i) large $E(2^+)$ values for very neutron rich nuclei (^{76}Ni and ^{80}Zn),
(ii) small B(E2) values in comparison to experimental values and for
(iii) ^{75}Cu, ^{77}Cu and ^{79}Cu the ground state is $3/2^-$ as compared to the experimental indication of $5/2^-$.
This may be due to neglect of the $f_{7/2}$ orbit for the protons. In view of this $f_{7/2}$ orbit has been included in the valence space of protons by taking ^{40}Ca as core. Effective interaction for fpg valence space for both protons and neutrons with ^{40}Ca as core has been constructed by Sorlin *et al.* [Sor02]. The main drawback of this interaction is that the effective proton single-particle energies of $f_{7/2}$ orbital becomes lower than $f_{5/2}$ which is not realistic. In the present work, we have modified two relevent matrix elements to account for this discrepancy.

7.1 Model space

In the present work we have used *fpg* model space comprising of the $0f_{7/2}$, $1p_{3/2}$, $0f_{5/2}$, $1p_{1/2}$ active proton orbitals and $0f_{7/2}$, $1p_{3/2}$, $0f_{5/2}$, $1p_{1/2}$, $0g_{9/2}$ neutron orbitals with

eight $f_{7/2}$ frozen neutrons, more accurately ^{40}Ca core with eight $f_{7/2}$ frozen neutrons. The single particle energies for $0f_{7/2}$, $1p_{3/2}$, $0f_{5/2}$, $1p_{1/2}$, $0g_{9/2}$ orbitals are 0.0, 2.0, 6.5, 4.0 and 9.0 MeV respectively. The relative single-particle energies are taken from the excitation energies of the low-lying negative parity states in ^{49}Ca [Sor02].

7.2 Effective Interaction

For the *fpg* valence space an effective interaction with ^{40}Ca as core has been reported in Ref. [Sor02]. This interaction has been built using *fp* two-body matrix elements (TBME) from Ref. [Pov01] and $1p_{3/2}$, $0f_{5/2}$, $1p_{1/2}$, $0g_{9/2}$ TBME from Ref. [Now96]. For the common active orbitals in these subspaces, matrix elements were taken from [Now96]. As the latter interaction has been defined for a ^{56}Ni core, a scaling factor of $A^{-1/3}$ amplitude is applied to take into account the change of radius between the ^{40}Ca and ^{56}Ni cores. As more and more neutrons are added in the $f_{7/2}$ shell, the excitation energy of the $9/2^+$ state decreases due to the attractive $\pi f_{7/2}\nu g_{9/2}$ interaction as reflected in Fig.7.1 for $^{41-71}$Sc isotopes. The remaining matrix elements are taken from $f_{7/2}g_{9/2}$ TBME from Ref. [Kah69].

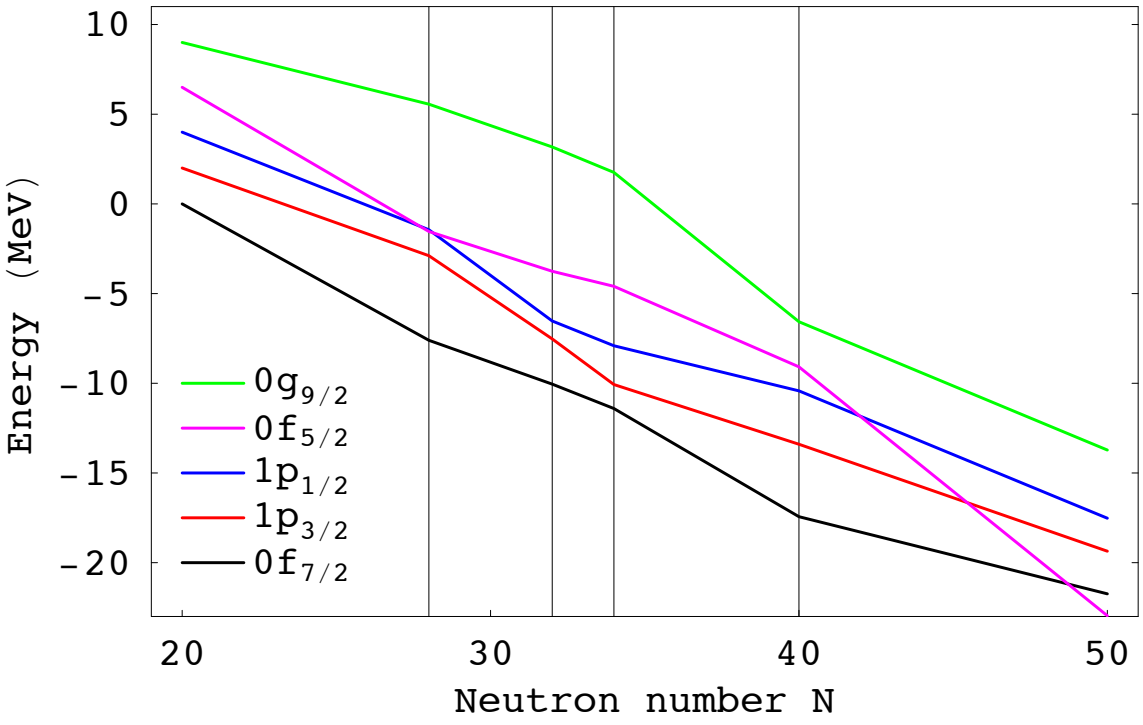

Figure 7.1: Effective proton single-particle energies in $^{41-71}$Sc isotopes using *pfg9* interaction.

7.3 Monopole correction

As more and more neutrons are added in $g_{9/2}$ orbital, $f_{7/2}$ orbital becomes more repulsive and $f_{5/2}$ more attractive. Thus proton $f_{5/2}$ is pulled down while $f_{7/2}$ is lifted up, as N increases, this is due to monopole interaction produced by tensor force between a proton in $j_{>,<} = l \pm 1/2$ and a neutron in $j'_{>,<} = l' \pm 1/2$. Effects on $p_{3/2}$ and $p_{1/2}$ orbitals are small and can be neglected. In the present work, we have modified $g_{9/2}f_{7/2}$ matrix elements by subtracting 100 KeV and $g_{9/2}f_{5/2}$ matrix elements by adding 100 KeV. This modified interaction is renamed as *pfg9a*. Effective single-particle energies for $^{41-71}$Sc isotopes is shown in Fig.7.2. The expression for effective proton-single particle energies are given in chapter 3.

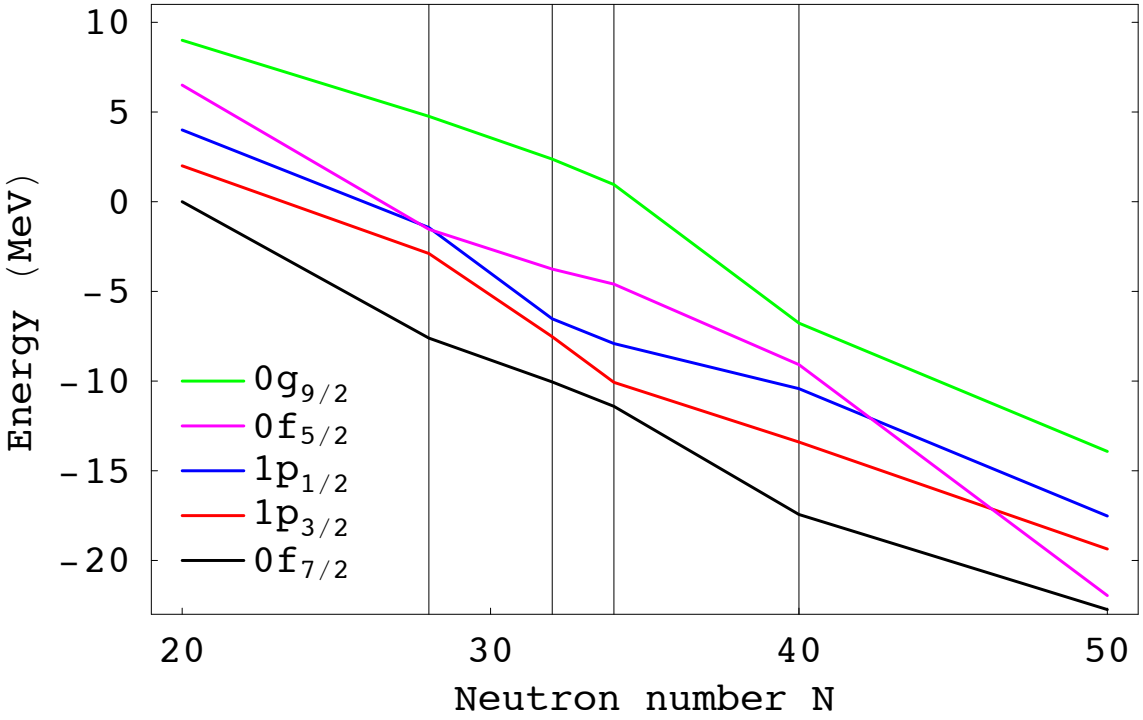

Figure 7.2: Effective proton single-particle energies in $^{41-71}$Sc isotopes using *pfg9a* interaction.

7.4 State of the art in the calculations

The modefied interaction has been tuned to reproduce the experimental data of Cu isotopes. These being odd nuclei the available experimental data is sparse. The aim of this tunning is to first reproduce the ground state properties of $^{75-79}$Cu and

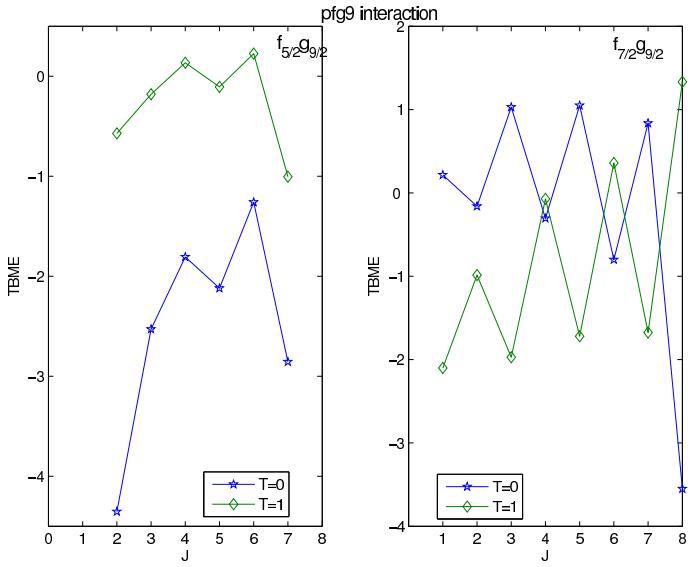

Figure 7.3: The changed TBME as a function of J for pfg9 interaction.

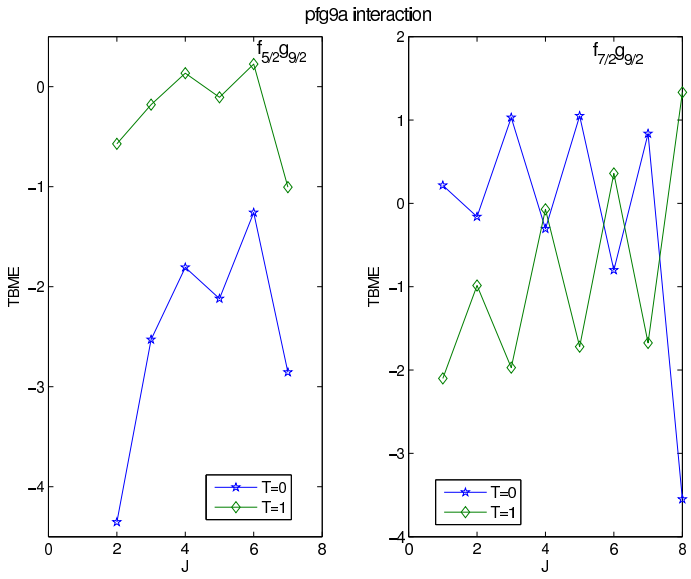

Figure 7.4: The changed TBME as a function of J for pfg9a interaction.

then apply it to Ni and Zn isotopes. In the original fpg interaction $f_{5/2}$ level crosses the $f_{7/2}$ at ^{70}Sc and become lower in energy. This appears to be unrealistic. In this modified interaction the $f_{7/2}$ effective single-particle energy is always lower than $f_{5/2}$ as expected. The original TBME of *pfg9a* interaction are shown in Fig. 7.3 and changed TBME for new interactionn *pfg9a* are shown in Fig. 7.4. Since the dimension of matrices involved for pfg9/2 space is very large, truncation of the full

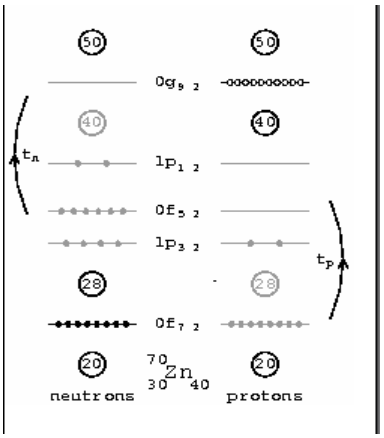

Figure 7.5: Model space and truncation, neutron: t_ν jumps from ($p_{3/2}$,$f_{5/2}$,$p_{1/2}$) to $g_{9/2}$, protons: t_π jumps from $f_{7/2}$ to ($p_{3/2}$,$f_{5/2}$,$p_{1/2}$) orbital .

shell-model space are necessary. We have allowed the following truncation neutron- t_ν jumps from (p_3, $f_{5/2}$, $p_{1/2}$) to $g_{9/2}$, protons- t_π jumps from $f_{7/2}$ to (p_3, $f_{5/2}$, $p_{1/2}$) orbital in each case, an example of this truncation are shown in Fig.7.5 for ^{7O}Zn isotope. For Cu, Ni and Zn nuclei the dimensions for different isotopes in m-scheme are tabulated in Table 7.1, 7.2 and 7.3. The calculations have been performed at SGI cluster computer at GANIL allowing highest feasible dimensions for each nucleus . Up to this dimension, the states seems to be more convergent, which can be taken as the final result.

7.5 Results and Discussions

The Yrast levels for the nickel, copper and zinc isotopes for $40 \leq N \leq 50$ are shown in Figs.7.6-7.8.

7.5.1 Copper isotopes

For ^{69}Cu, the ground state $3/2^-$ is well predicted by *fpga* interaction. The calculated $1/2^-$ and $5/2^-$ state is reverse in comparison to experimental levels. The calculated $1/2^-$ and $5/2^-$ state is at 134 KeV and at 378 KeV lower in energy from the experimental levels. The order of $7/2^-_1$, $7/2^-_2$ and $9/2^-$ is well reproduced by this interaction. The $7/2^-_2$ is only 62 KeV below then experimental value. In ^{69}Cu the $3/2^-$ is interpreted by $\pi p_{3/2}$, the $5/2^-$ is interpreted by $\pi p_{5/2}$. The first $7/2^-$ is interpreted by $\pi p_{3/2} \otimes 2^+(^{68}\text{Ni})$ and the second $7/2^-$ is interpreted by $\pi p^{-1}_{7/2}$.

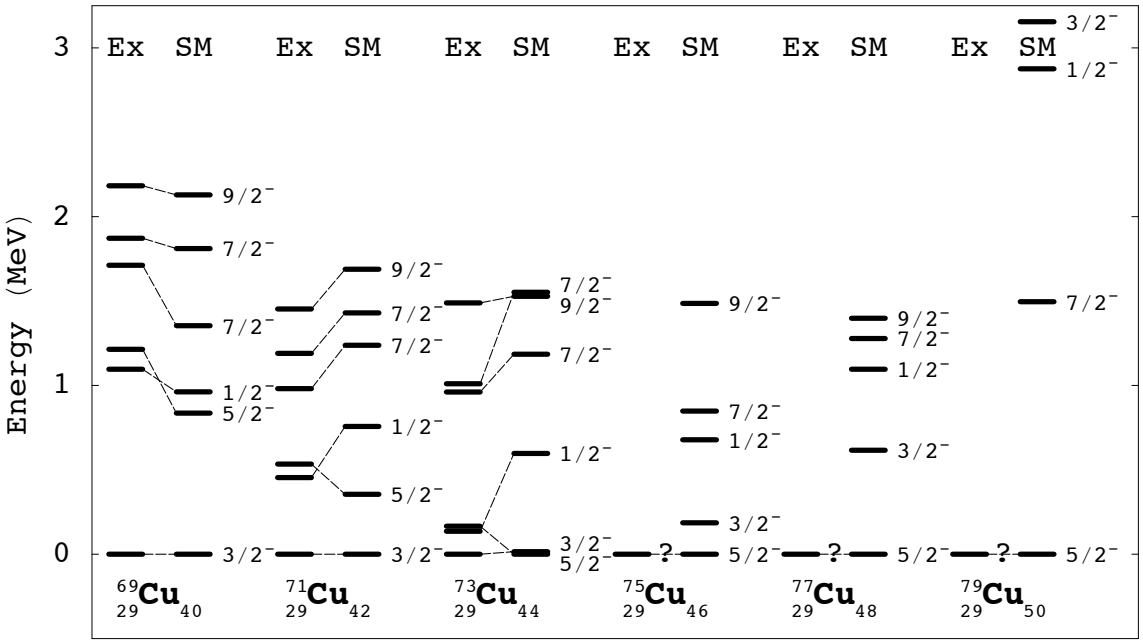

Figure 7.6: Yrast levels of $^{69-79}$Cu isotopes with pfg9a interaction.

For ^{71}Cu, the ground state $3/2^-$ is well predicted by *fpg9a* interaction. The order of $5/2^-$ and $1/2^-$ state is reverse in comaprison to experimental levels. The calculated $1/2^-$ level is 303 KeV higher than the experimental value, while $5/2^-$ level is 179 KeV lower than the experimental result. The order of $7/2^-_1$, $7/2^-_2$ and $9/2^-$ is well reproduced and are higher in energy from the experimental values. In the ^{71}Cu, the $3/2^-$ is interpreted by $\pi p_{3/2}$, and the $5/2^-$ is interpreted by $\pi p_{5/2}$. The first $7/2^-$ is interpreted by $\pi p_{3/2} \otimes 2^+(^{70}\text{Ni})$ and the second $7/2^-$ is interpreted by $\pi p^{-1}_{7/2}$.

For ^{73}Cu, *fpg9a* interaction predicts $5/2^-$ state lower in energy by 15 KeV from $3/2^-$ state while experimentally $3/2^-$ is ground state. The $1/2^-$ state is 462 KeV higher in energy from experimental value. The $9/2^-$ state lies in between two $7/2^-$ states. In the ^{73}Cu, the $3/2^-$ is interpreted by $\pi p_{3/2}$, and the $5/2^-$ is interpreted by $\pi p_{5/2}$. The first $7/2^-$ is interpreted by $\pi p_{3/2} \otimes 2^+(^{72}\text{Ni})$ and the second $7/2^-$ is interpreted by $\pi p^{-1}_{7/2}$.

Recently, there is an experimental indication of $5/2^-$ as a ground state in ^{75}Cu at REX-ISOLDE, CERN [Fla09]. The *fpga* interaction also predicts $5/2^-$ as a ground state. For ^{77}Cu and ^{79}Cu, this interaction predicts $5/2^-$ as a ground state which is also expected from experiment. The calculations predict that the $1/2^-$, $9/2^-$ and

$7/2^-$ states are at very high in energy for ^{79}Cu isotopes.

7.5.2 Nickel isotopes

The nickel isotopes (Z=28) cover three doubly-closed shells with number N=28, N=40, N=50 and therefore serve as a unique testing ground for large scale shell model calculations. Experimentally, the 8^+ isomerism though expected to be present in a whole chain from ^{72}Ni to ^{76}Ni was found to be suddenly absent in ^{72}Ni and ^{74}Ni and present in ^{70}Ni and ^{76}Ni. The ground state spin from ^{68}Ni to ^{76}Ni is correctly reproduced by *fpg9a* interaction.

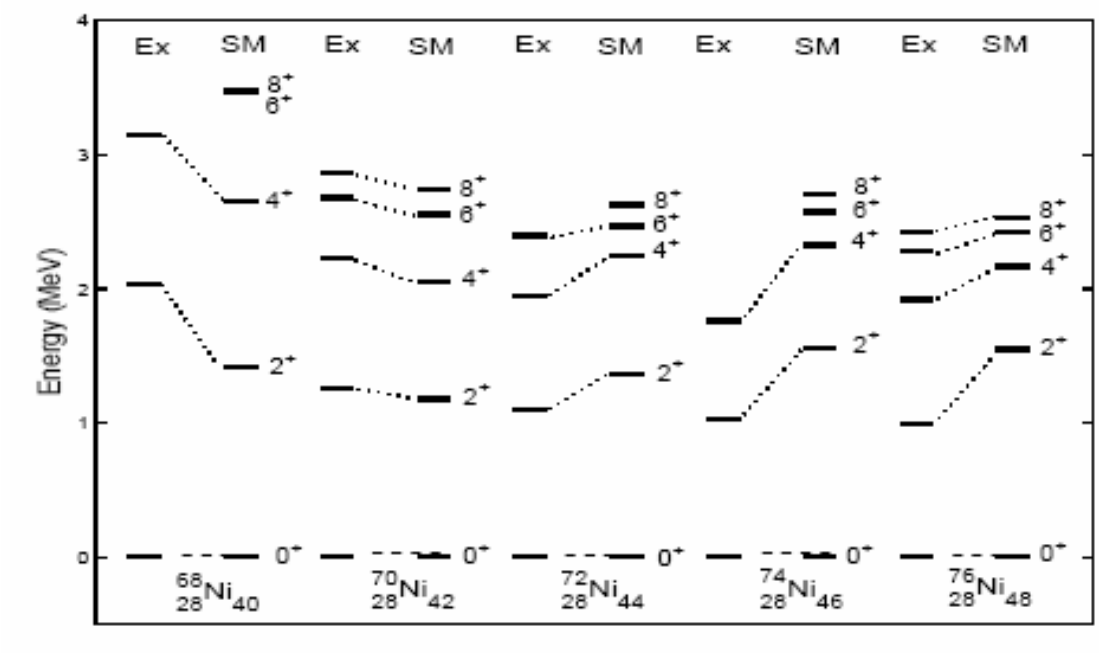

Figure 7.7: Yrast levels of $^{68-76}$Ni isotopes with pfg9a interaction.

For ^{70}Ni, the first excited state 2^+ is calculated at 1.26 MeV which is 80 KeV below the experimental level. The states 4^+ at 2.68 MeV, 6^+ at 3.47 MeV, and 8^+ at 3.48 MeV are well predicted at 2.23 MeV, 2.68 MeV and 2.86 MeV. The agreement with the experimental data is excellent. For ^{72}Ni the first excited state 2^+ is calculated at 1.36 MeV which is 266 KeV above the experimental level. The states 4^+ at 1.94 MeV and 6^+ at 2.34 MeV are well predicted at 2.25 MeV and 2.47 MeV. Theoretically, there is 8^+ state at 2.62 MeV but experimentally their is no indication of 8^+ isomeric states. For ^{74}Ni, only two excited states are experimentally known. The first excited state 2^+ is calculated at 1.56 MeV which is 533 KeV above the experimental value. The state 4^+ at 1.76 MeV is predicted at 2.32 MeV. The

calculated 6^+, 8^+ states are at 2.57 MeV and 2.70 MeV respectively. For ^{76}Ni, the calculated first 2^+ state is slightly higher in energy about 557 KeV from the experimental value. The states 4^+ at 1.92 MeV, 6^+ at 2.28 MeV and isomeric states 8^+ at 2.42 MeV are well predicted at 2.17 MeV, 2.42 MeV and 2.53 MeV. The agreement for 4^+, 6^+ and 8^+ states with the experiment is excellent.

7.5.3 Zinc isotopes

The ground state spin for $^{70-80}$Zn isotopes for $40 \leq N \leq 50$ is correctly reproduced by *fpga* interaction. For ^{70}Zn, the first excited 2^+ state is calculated at 0.603 MeV which is 282 KeV below the experimental value. The states 4^+ at 1.79 MeV, 6^+ at 2.89 MeV and 8^+ at 3.75 MeV are well predicted at 1.47 MeV, 2.37 MeV and 2.53 MeV respectively. The calculated values are compressed in comparison to the experimental value. For ^{72}Zn, experimentally only 2^+ state at 0.653 MeV is known, which is predicted well by *fpga* interaction with energy difference of 74 KeV. The calculated values of states 4^+, 6^+ and 8^+ are at 1.178, 1.923 and 2.601 MeV respectively. For ^{74}Zn, the first excited 2^+ state is calculated at 0.825 MeV which is 219 KeV above the experimental value. The states 4^+ at 1.419 MeV is predicted at 1.551 MeV. The states 6^+ and 8^+ are at 2.783 MeV and 3.430 MeV. For ^{76}Zn, the first excited 2^+ state is calculated at 0.997 MeV which is 398 KeV above the experimental value. The first 4^+ state is calculated with energy difference of 679 KeV from the experimental value. The calculated 4^+, 6^+ and 8^+ states are at 1.975 MeV, 3.036 MeV and 3.243 MeV respectively. For ^{78}Zn the first excited 2^+ state is calculated at 1.307 MeV, which is 477 KeV above the experimental value. The states 4^+ at 1.621 MeV, 6^+ at 2.528 MeV and 8^+ at 2.673 MeV are predicted at 2.247 Mev, 2.923 MeV and 2.955 MeV. Experimentally, the difference between 6^+ and 8^+ states is 145 KeV while theoretically, it is only 32 KeV. For ^{80}Zn the first excited 2^+ state is calculated at 1.953 MeV which is 461 KeV smaller than the experimental value.

The calculated and experimental $E(2_1^+)$ and $E(4_1^+)$ for Ni and Zn isotopes are shown in Fig. 7.9. The high values of $E(2_1^+)$ for Ni at N=40 is an indication of shell closure at N=40. For Zn isotopes, the $E(2_1^+)$ and $E(4_1^+)$ at N=40 and 50 are high in comparison to neighbouring isotopes reflecting shell closure at N=40 and N=50.

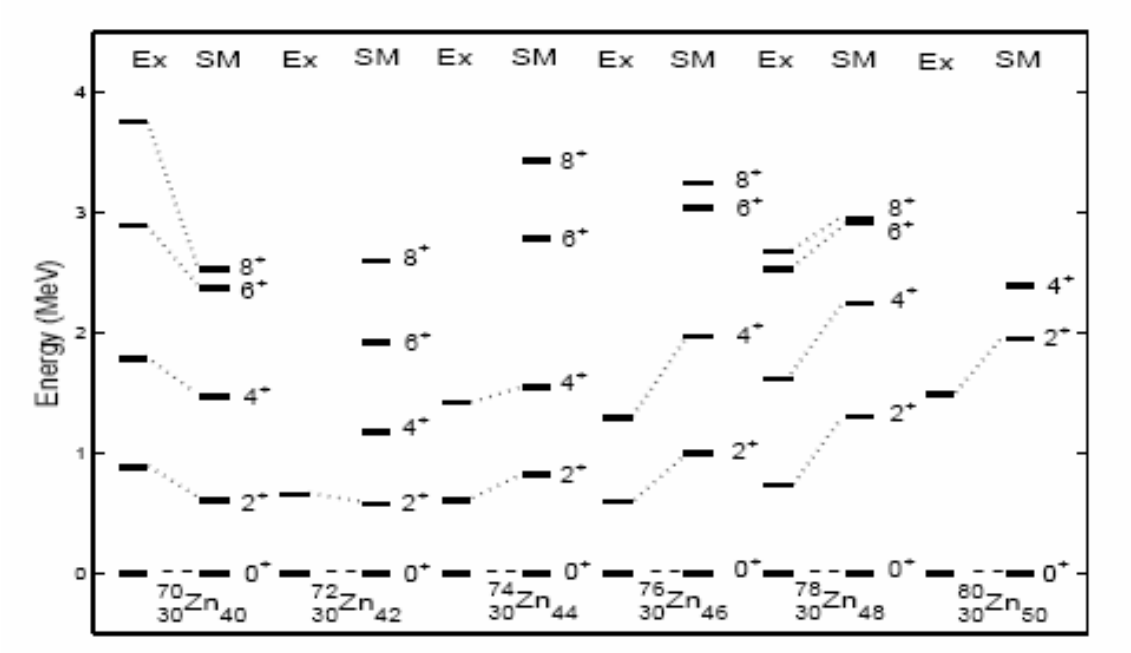

Figure 7.8: Yrast levels of $^{70-80}$Zn isotopes with pfg9a interaction.

7.5.4 The B(E2) systematics in the copper isotopes

The calculated values of first excited states of $1/2^-$, $5/2^-$ and $7/2^-$ with its corresponding experimental values are shown in Fig. 7.10 for $^{69-79}$Cu isotopes. In the lower part of this figure, the calculated and experimental B(E2) values corresponding to different transitions namely, B(E2;$1/2^- \rightarrow 3/2^-$), B(E2;$1/2^- \rightarrow 3/2^-$) and B(E2;$1/2^- \rightarrow 3/2^-$) are also shown. The calculated and experimental B(E2) values are tabulated in Table 7.4. The previously calculated value by Stefanescu *et al.* are shown within bracket [Ste08]. The calculated B(E2;$1/2^- \rightarrow 3/2^-$) values show much better agrreement with experimental data compared to those of earlier work of Stefanescu [Ste08]. The low B(E2) value beyond N=40 for $5/2^-$ state confirms its $\pi f_{5/2}$ single particle charactor. The sharp drop in the excitation energy of $5/2^-$ state beyond N=40 could be due to the monopole migration. The large B(E2)value for $1/2^-$ state depart it from the single-particle charactor of $\pi p_{1/2}$ type.

7.5.5 The B(E2) systematics in the nickel isotopes

The B(E2;$2_1^+ \rightarrow 0_{gs}^+$) value in ^{68}Ni is much lower as compared to ^{56}Ni. This low value was interpreted by Sorlin *et al.* [Sor02] as orginating from the enhanced neutron pair scattering at N=40 which is referred to as superfluid behaviour of the neutrons.

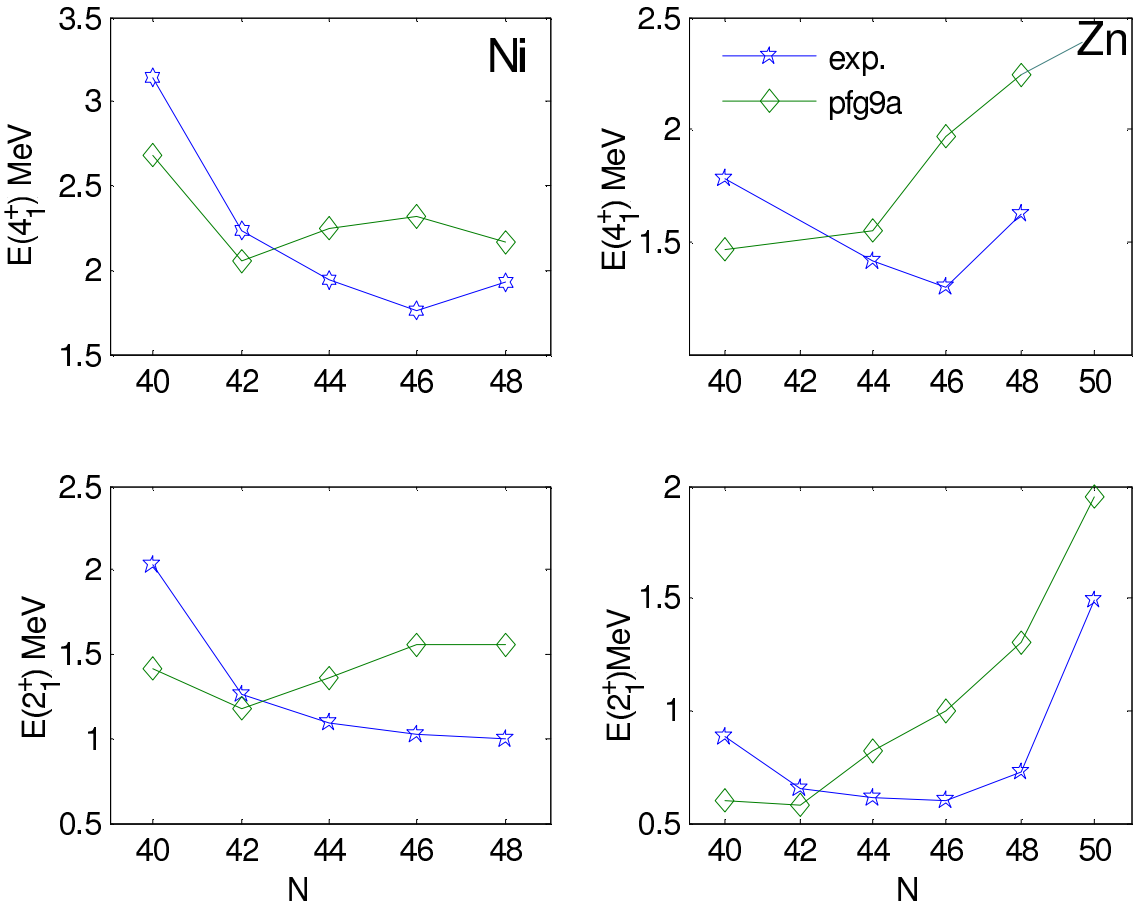

Figure 7.9: The calculated and experimental E(2_1^+) and E(4_1^+) for Ni and Zn isotopes as a function of neutron number .

The constancy of the B(E2) values beyond $N = 40$ can be understood as follows: *E2* strength as $np - nh$ excitation across $N = 40$ for odd n cannot contribute due to parity conservation and for even n are dominated by pair scattering. Langanke *et al.* [Lan03] performed microscopic calculations of the B(E2) in even-even nickel isotopes and found that the small observed B(E2) value is not necessarily an argument for a shell closure at N=40, but it simply reflects the fact that the lowest 2^+ state in ^{68}Ni is primarily a neutron excitation. Van de Walle *et al.* [Wal07] showed that B(E2) values in the Ni chain show a parabolic evolution between two magic numbers N=28 and 40, hinting a seniority-like behaviour . Peru *et al.* [Per06] measured high B(E2) value for ^{70}Ni at GANIL, and attributed it due to rapid proton core polarization when neutrons are added to the $g_{9/2}$ orbit . The calculated B(E2;$2_1^+ \rightarrow 0_{gs}^+$) for $^{68-76}$Ni are shown in Fig. 7.11, the B(E2) value is almost constant from ^{68}Ni to ^{74}Ni and its value again decreases for ^{76}Ni. This decrease in B(E2) value is probably due

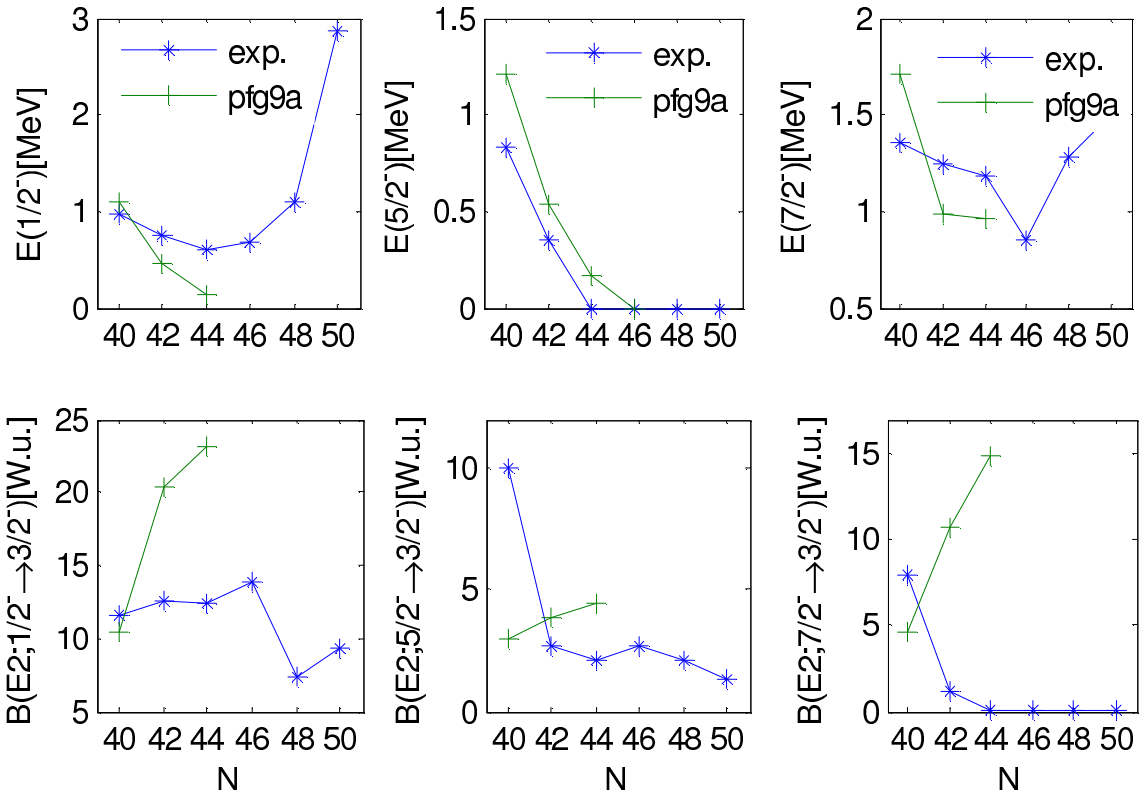

Figure 7.10: The excited energy and B(E2) for $^{69-79}$Cu istopes .

to oncoming of the next shell closure at N=50 for ^{78}Ni.

7.5.6 The B(E2) systematics in the zinc isotopes

The experimental B(E2;$2_1^+ \rightarrow 0_{gs}^+$) values in the Zn isotopic chain show a similar trend towards $N = 40$ as the Ni isotopes up to ^{68}Zn, though for ^{70}Zn (at N = 40), the B(E2) value suddenly increases. Leesshardt *et al.* [Lee02] give three effects for supporting this increased collectivity: the addition of two protons out of the Ni core, the maximum in neutron pairing correlations at $N = 40$, and the presence of the strongly downsloping $l = 4$ Nilsson neutron orbitals close to the Fermi surface. Kenn *et al.* [Ken02] indicate that the inclusion of the $g_{9/2}$ orbit in the valence space is important in order to reproduce the increased B(E2;$2_1^+ \rightarrow 0_{gs}^+$) values in the ^{70}Zn.

The calculated B(E2;$2_1^+ \rightarrow 0_{gs}^+$) values in present work obtained using *fpg9a* interaction for $^{70-80}$Zn are shown in Fig. 7.11. The calculated value show similar trends as experimental values from ^{70}Zn to ^{80}Zn. The B(E2) value at N=50 is very low, this is an indication of shell closure at N=50.

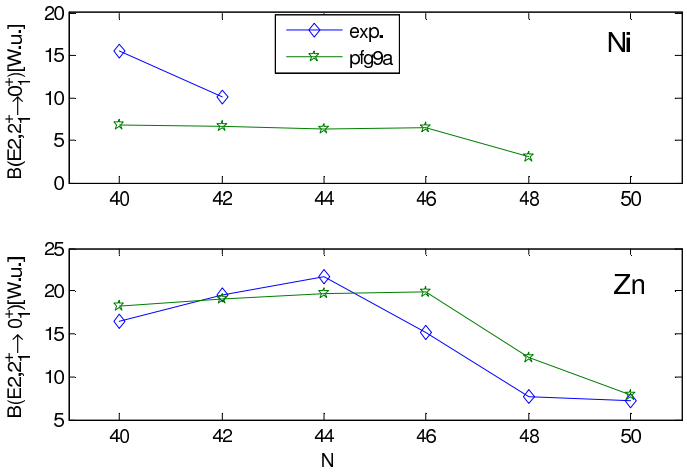

Figure 7.11: The calculated and experimental B(E2;$_1^+ \rightarrow 0_{gs}^+$)in W.u. for Ni and Zn isotopes as a function of neutron number .

7.6 Conclusion

In the present work, the exsisting pfg9 interaction for fpg shell with ^{40}Ca core has been modified by changing $\pi f_{5/2}\nu g_{9/2}$ and $\pi f_{7/2}\nu g_{9/2}$ matrix elements. The new interaction named as pfg9a has been tuned for Cu isotopes and tested for Ni and Zn isotopes. The *fpg9a* interaction predicts ground state spin as 0^+ for all even even isotopes of Ni and Zn considered here, as is the characteristic of any acceptable interaction. These results indicate that further modification in interaction and inclusion of $1d_{5/2}$ orbit is important in the shell model calculations.

Table 7.1: M-scheme dimensions as a function of jumps for $^{69-79}$Cu isotopes.

^{69}Cu	$t_\nu = 0$	2	4	6	8	10
t_π=0	**3**	**3015**	**91491**	**254913**	**276525**	**276653**
=2	**696**	**1 373609**	**43 848479**	122 508489	132 506724	132 548241
=4	**8278**	**17 416837**	56 220177	1571 756217	1698 900750	1699 403878
=6	**15182**	**31 846516**	1027 361104	2872 107718	3104 553769	3105 475749
=8	**15666**	**32 741114**	1055 656178	2951 119519	3190 611915	3191 011443
^{71}Cu	$t_\nu = 0$	2	4	6	8	10
t_π=0	**50**	**12240**	**100716**	**140505**	**141327**	-
=2	**21919**	**5 825341**	**48 300211**	66 786991	67 82029	-
=4	**276441**	74 558999	619 343936	854 648994	858 257760	-
=6	**505615**	136 261373	1131 775961	1561 940288	1568 550518	-
=8	**519955**	140 025730	1162 940794	1605 106425	1611 915579	-
^{73}Cu	$t_\nu = 0$	2	4	6	8	10
t_π=0	**196**	**12386**	**33998**	**35467**	-	-
=2	**91796**	**5 895218**	**15 893453**	**16 434926**	-	-
=4	**1 170549**	75 453107	202 597640	209 239245	-	-
=6	**2 139687**	137 895445	370 341496	382 505434	-	-
=8	**2 199186**	141 704961	380 646633	393 174584	-	-
^{75}Cu	$t_\nu = 0$	2	4	6	8	10
t_π=0	**196**	**3208**	**4030**	-	-	-
=2	**91796**	**1 464709**	**1 759747**	-	-	-
=4	**1 170549**	**18 579108**	**22 187874**	-	-	-
=6	**2 139687**	**33 971021**	**40 581251**	-	-	-
=8	**2 199186**	**34 924634**	**41 733788**	-	-	-
^{77}Cu	$t_\nu = 0$	2	4	6	8	10
t_π=0	**50**	**178**	-	-	-	-
=2	**21919**	**63436**	-	-	-	-
=4	**276441**	**779569**	-	-	-	-
=6	**505615**	**1 427595**	-	-	-	-
=8	**519955**	**1 470207**	-	-		-
^{79}Cu	$t_\nu = 0$	2	4	6	8	10
t_π=0	**3**	-	-	-	-	-
=2	**696**	-	-	-	-	-
=4	**8278**	-	-	-	-	-
=6	**15182**	-	-	-	-	-
=8	**15666**	-	-	-	-	-

Table 7.2: M-scheme dimensions as a function of jumps for $^{68-78}$Ni isotopes.

^{68}Ni	$t_\nu = 0$	2	4	6	8	10
t_π=0	1	267	7899	21983	23870	23884
=2	213	406511	12 925115	36 103205	39 058892	39 071390
=4	4589	9 559885	308 102401	861 287533	931 046542	931 324322
=6	11233	23 351077	752 169445	2102 592191	2272 962812	2273 642652
=8	12022	24 809156	798 311744	2231 445092	3190 611915	2413 129934
^{70}Ni	$t_\nu = 0$	2	4	6	8	10
t_π=0	5	1061	8693	12159	12240	-
=2	6505	1 718215	14 236819	19 700103	19 788576	-
=4	276441	40 870755	339 413271	468 498987	470 488980	-
=6	505615	99 786111	828 604479	1143 853373	1148 721926	-
=8	519955	105 924344	879 426932	1214 239804	1219 431970	-
^{72}Ni	$t_\nu = 0$	2	4	6	8	10
t_π=0	18	1074	2961	3103	-	-
=2	27122	1 738832	4 694519	4 856715	-	-
=4	642040	41 360922	111 119931	114 781029	-	-
=6	1 567792	100 982860	271 353481	280 309389	-	-
=8	1 664802	107 194732	288 153754	297 701914	-	-
^{74}Ni	$t_\nu = 0$	2	4	6	8	10
t_π=0	18	284	365	-	-	-
=2	27122	433420	521893	-	-	-
=4	642040	10 197336	12 187329 -	-	-	
=6	1 567792	24 907636	29 776189	-	-	-
=8	1 664802	26 461936	31 654102	-	-	-
^{76}Ni	$t_\nu = 0$	2	4	6	8	10
t_π=0	5	19	-	-	-	-
=2	6505	19003	-	-	-	-
=4	151873	429653	-	-	-	-
=6	371043	1 050883	-	-	-	-
=8	394414	1 120234	-	-		-
^{78}Ni	$t_\nu = 0$	2	4	6	8	10
t_π=0	1	-	-	-	-	-
=2	213	-	-	-	-	-
=4	4589	-	-	-	-	-
=6	11233	-	-	-	-	-
=8	12022	-	-	-	-	-

Table 7.3: M-scheme dimensions as a function of jumps for $^{70-80}$Zn isotopes.

^{70}Zn	$t_\nu = 0$	2	4	6	8	10
t_π=0	**14**	**16128**	**493350**	**1 375124**	**1 491044**	**1 491684**
=2	**1612**	**3 194842**	102 117490	285 328090	308 590222	308 686306
=4	**11562**	**24 234706**	781 885318	2185 865224	2362 756684	2363 458206
=6	**17056**	**35 651958**	1149 600366	3213 756866	3473 946344	3474 980444
=8	**17276**	**36 049132**	1162 118680	3248 706216	3511 776876	3512 823738
^{72}Zn	$t_\nu = 0$	2	4	6	8	10
t_π=0	**266**	**65948**	**543170**	**756736**	**760942**	-
=2	**50964**	**13 563790**	112 486438	155 502722	156 186110	-
=4	**384786**	103 701728	861 352340	1188 710006	1193 739404	-
=6	**566208**	152 485426	1266 433834	1747 922052	1755 332922	-
=8	**572586**	154 151756	1280 221304	1767 031262	1744 531610	-
^{74}Zn	$t_\nu = 0$	2	4	6	8	10
t_π=0	**1056**	**66738**	**182658**	**190220**	-	-
=2	**213672**	**13 726498**	**36 988630**	**38 243190**	-	-
=4	**1 628418**	104 945360	281 836820	291 091742	-	-
=6	**2 394904**	154 314122	414 503600	428 139198	-	-
=8	**2 421274**	156 000444	419 071104	432 870264	-	-
^{76}Zn	$t_\nu = 0$	2	4	6	8	10
t_π=0	**1056**	**17170**	**21376**	-	-	-
=2	**213672**	**3 406902**	**4 090290**	-	-	-
=4	**1 628418**	**25 851562**	**30 880960**	-	-	-
=6	**2 394904**	**38 029806**	**45 440676**	-	-	-
=8	**2 421274**	**38 453130**	**45 953478**	-	-	-
^{78}Zn	$t_\nu = 0$	2	4	6	8	10
t_π=0	**266**	**906**	-	-	-	-
=2	**50964**	**147048**	-	-	-	-
=4	**384786**	**1 086308**	-	-	-	-
=6	**566208**	**1 600308**	-	-	-	-
=8	**572586**	**1 619448**	-	-		-
^{80}Zn	$t_\nu = 0$	2	4	6	8	10
t_π=0	**14**	-	-	-	-	-
=2	**1612**	-	-	-	-	-
=4	**11562**	-	-	-	-	-
=6	**17056**	-	-	-	-	-
=8	**17276**	-	-	-	-	-

Table 7.4: B(E2) value for $^{69-79}$Cu isotopes . The results in the bracket from earlier work of Stefanescu *et al*. [Ste08].

	^{69}Cu		^{71}Cu		^{73}Cu		^{75}Cu	^{77}Cu		^{79}Cu
	Expt.	fpg9a	Expt.	fpg9a	Expt.	fpg9a	Expt.	fpg9a	Expt.	fpg9a
B(E2;1/2-→ 3/2-)	10.4	11.5(7.1)	20.4	12.4(7.3)	23.1	12.41(7.5)	13.8	7.3		9.2
B(E2;5/2-→ 3/2-)	3.0	9.9(1.6)	3.9	2.6(1.7)	4.4	2.07(1.3)	2.6	2.1		1.3
B(E2;7/2-→ 3/2-)	4.6	7.9(1.2)	10.7	1.1(1.5)	14.9	0.0044(2.3)	0.0032	0.000002		0.0017